

Conducting Wall Hall Thrusters

Dan M. Goebel¹, Richard R. Hofer², Ioannis G. Mikellides³, Ira Katz⁴, James E. Polk⁵ and Brandon Dotson⁶
Jet Propulsion Laboratory, California Institute of Technology, Pasadena, CA 91109

A unique configuration of the magnetic field near the wall of Hall thrusters, called “Magnetic Shielding”, has recently demonstrated the ability to significantly reduce the erosion of the boron nitride (BN) walls and extend the life of Hall thrusters by orders of magnitude. The ability of magnetic shielding to minimize interactions between the plasma and the discharge chamber walls has for the first time enabled the replacement of insulating walls with conducting materials *without* loss in thruster performance. The boron nitride rings in the 6 kW H6 Hall thruster were replaced with graphite that self-biased to near the anode potential. The thruster efficiency remained over 60% (within two percent of the baseline BN configuration) with a small decrease in thrust and increase in I_{sp} typical of magnetically shielded Hall thrusters. The graphite wall temperatures decreased significantly compared to both shielded and unshielded BN configurations, leading to the potential for higher power operation. Eliminating ceramic walls makes it simpler and less expensive to fabricate a thruster to survive launch loads, and the graphite discharge chamber radiates more efficiently which increases the power capability of the thruster compared to conventional Hall thruster designs.

Nomenclature

g	=	acceleration of gravity
I_{sp}	=	specific impulse
\dot{m}_p	=	total propellant mass flow rate
T	=	thrust
P_T	=	Total input power
P_d	=	Discharge power
P_{mag}	=	Power into the magnets

I. Introduction

High-power, highly throttleable electric propulsion (EP) enables a significant number of very challenging, high Δv missions by increasing the delivered payload mass and providing rapid transit times relative to other existing propulsion technologies [1,2]. Hall thrusters are the prime candidate for many future missions because of their higher thrust and lower cost compared to traditional ion thrusters [3,4]. Every Hall thruster fabricated today in the US and Europe has dielectric walls made of either boron nitride (BN) or BNSiO₂ [5], or segmented walls that contain both carbon and ceramic material typically in a layered structure[6-8]. This is because these ceramic materials provide:

- 1) Insulating surfaces so as to not short out the electric field in the thruster acceleration region,
- 2) Low sputtering yield under ion bombardment to minimize the erosion and extend thruster life,
- 3) Low secondary electron yield to minimize the electron power loss to the wall.

Hall thrusters that use other wall materials such as higher secondary electron yield ceramics (Al₂O₃, SiC, macor, etc.), or conductors (graphite, carbon velvet, stainless steel, etc.) [9-12] are significantly less efficient and are

¹ Senior Research Scientist, Jet Propulsion Laboratory, California Institute of Technology, Fellow AIAA

² Senior Engineer, Electric Propulsion Group, Jet Propulsion Laboratory, Associate Fellow AIAA

³ Principal Engineer, Electric Propulsion Group, Jet Propulsion Laboratory, Associate Fellow AIAA

⁴ Group Supervisor, Electric Propulsion Group, Jet Propulsion Laboratory, Member AIAA

⁵ Principal Engineer, Electric Propulsion Group, Jet Propulsion Laboratory, Associate Fellow AIAA

⁶ Graduate Student, California Institute of Technology, Pasadena, CA

predicted to have shorter life times and lower throughput capabilities. The poorer performance of thrusters using alternative materials has been largely attributed to the higher secondary yield [13-15] of these materials compared to the standard BN.

Shortly after the discovery that the erosion of the BN walls in the BPT-4000 Hall thruster had essentially stopped after 5,600 hours of operation during life-testing [16], an extensive investigation into the mechanism responsible for this effect was initiated at JPL [17,18]. The erosion of the boron nitride wall occurs due to sputtering of the surface by energetic ion bombardment from the plasma in the thruster. The rate of erosion is determined by the energy of the ions, the angle of incidence of the ions, and the flux of ions onto the surface. It was found that the BPT-4000 had experience erosion of the BN walls until a certain magnetic field topology was exposed close to the walls near the thruster exit plane that significantly reduced the energy and flux of the ions hitting the wall. This effect has been named “magnetic shielding” [17] and reproduced by modifying another laboratory Hall thruster at JPL to produce the correct magnetic topology at the wall [19]. Extensive theoretical and experimental efforts have gone into explaining magnetic shielding physics and demonstrating that this effect reduces the erosion of the boron nitride walls by a much as a factor of 1000 [20-22].

Magnetic shielding significantly reduces the plasma contact with the wall. Experiments on a modified H6 Hall thruster with BN walls at JPL [20] demonstrated that this reduced contact and low wall erosion was achieved with less than 2% change in the thruster efficiency. While the total efficiency was largely unchanged, the thrust was reduced and the Isp increased relative to the baseline performance. The thrust decrease was found to be due to plume divergence angle increases in the magnetically shielded configuration due to the field shape and movement of the plasma downstream by a few millimeters. The Isp increase was found to be due to a larger amount of higher ionized ions in the plume, which increase the ion velocity and therefore the Isp. After testing, the magnetically shielded H6 BN walls were found to be no longer kept clean from ion sputtering, but were coated with a thin layer of backspattered carbon from the beam dump. These experiments demonstrated both the reduced erosion of the dielectric surface due to the magnetic field structure, and that the thruster performance was not significantly affected by the presence of a somewhat resistive surface in contact with the plasma due to the thin carbon deposition layer.

To determine if fully conducting walls could be implemented in Hall thrusters, the Magnetically Shielded H6 Hall thruster was retrofitted with new walls fabricated of graphite. The H6 thruster is designed with replaceable “rings” near the thruster exit plane where the plasma contacts the walls to provide the ability to measure the erosion rate by removing these rings and measuring the surface profile on precision CMM machines. The selection of graphite as the material for the rings is because it features a low secondary electron yield, a very high emissivity to efficiently radiate any deposited power, and has good strength and a reduced mass compared to stainless steel. Tests at the nominal 6 kW power level of the H6 thruster showed that the fully conductive graphite rings reduced the total thruster efficiency slightly to about 60.5%. The slight difference with magnetic shielding between the graphite wall and the boron nitride wall is not considered significant, and it is probable that further optimization not possible within the limited testing time available to date will make up these small differences.

The reduced plasma contact with the wall is visually illustrated by the photos shown in Fig. 1 of the unshielded H6 on the left and the magnetically shielded graphite wall H6 on the right, both operating at the same discharge power level of 6 kW. There is a clear visual gap in the magnetically shielded thruster between the wall and the plasma indicative of low excitation and suggesting a detached plasma condition. Detailed probe measurements of this region [18,20] show low electron temperatures and plasma potentials near the anode potential, which significantly reduce the ion energy striking the wall and reduce the erosion rates. Thermal imaging of the graphite rings, the walls and anode also show a significant decrease in the surface temperature and radiated power at the nominal operating power level. Given this decrease in radiated power as well as the decrease in ring, wall, and anode temperatures observed at even higher operating powers than the nominal 6 kW, it is likely that the use of magnetic shielding techniques and graphite discharge chambers will result in higher power density capabilities in future Hall thrusters of this design.

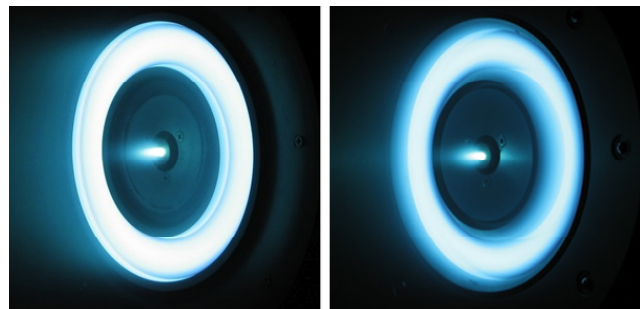


Figure 1. Photograph of the unshielded H6 thruster (left) and magnetically shielded H6 thruster with graphite rings (right) suggesting reduced plasma contact with the walls.

It is important to recognize that the configuration discussed in this paper is not a so-called “Thruster with Anode Layer” (TAL). A TAL has a similar basic magnetic field configuration as an insulating-wall Hall thruster but with a different electrode design [5]. While a TAL has a discharge region where the transverse magnetic field lines terminate directly on metallic walls, these walls are usually biased to cathode potential or float close to cathode potential in order to minimize electron energy loss. The significant plasma contact with the metallic walls compresses the acceleration region close to the anode (giving it the acronym “anode layer thruster”). The conducting-wall Hall thruster described here has the same geometry as a traditional BN-wall Hall thruster with a deeper channel and near-zero transverse B-field close to the anode. This eliminates the anode power loading problems often observed in TAL thrusters, and provides the near-zero wall erosion of a magnetically shielded thruster.

The replacement of traditional ceramic walls with graphite, enabled by the recently discovered magnetic shielding, represents a major advance in Hall Thruster technology. This advance greatly simplifies construction of the thruster required to withstand launch vibrations by eliminating large fragile ceramics and their support structures, and will thereby lead to significant reductions in the thruster mass and cost. The new design could also lead to factors of two to three increase in the thruster power density due to the lower power loading on the walls and higher emissivity surfaces, resulting in ultra-compact, very long life Hall thrusters for space missions.

II. Experimental Apparatus

The results presented here are from experiments on the 6-kW H6 Hall thruster [23] that uses an on-axis lanthanum hexaboride hollow cathode designed specifically for this thruster [24]. The thruster was a joint development between AFRL, JPL and the University of Michigan [23, 25-28]. The data collected on this thruster at JPL is used to validate plasma simulations [18,22,29] intended to evaluate thrusters being considered for NASA science missions. Details on the experimental configuration and thruster performance can be found in Refs. [20,30] and the original references. The nominal operating characteristics of the H6 thruster at 6 kW and 300 V in the unshielded BN-wall configuration are found in Table 1.

The experiments were conducted in a 3-m-dia. by 10-m-long vacuum chamber at JPL that was used for the 30,000 hour Extended Life Test of the NSTAR ion thruster [31]. A photograph of the thruster on the thrust stand in the chamber is shown in Fig. 2. The vacuum chamber has a total xenon system pumping speed of approximately 200,000 l/s and produces a background pressure of 1.6×10^{-5} torr at the nominal xenon flow rate of about 21 mg/s at the 6kW operation point. At this background pressure, ingestion from background gases is negligible [32]. The vacuum chamber is lined with graphite panels to reduce the amount of back sputtered material on the thruster and diagnostics. Commercially available power supplies and flow controllers are used to operate the thruster. The propellant flow

Table 1. Nominal operating conditions for the 6 kW laboratory Hall thruster with the internal cathode.

Parameter	Value
Discharge Voltage (V)	300.0
Discharge Current (A)	20.0
Anode Flow Rate (mg/s)	20.0
Nominal Cathode Flow Rate (mg/s)	1.34
Nominal Cathode to Ground Voltage	-10.8
Nominal Cathode Coupling Voltage	19.6
Ion Current Fractions (plume averaged)	Xe ⁺ = 0.75 Xe ⁺⁺ = 0.18 Xe ⁺⁺⁺ =0.07
Average Plume Divergence (half angle, defined in Ref. [25])	19°
Nominal Thrust (mN)	392 ±2
Total Efficiency	61-63%
Vacuum Chamber Pressure (Torr)	1.6×10^{-5}

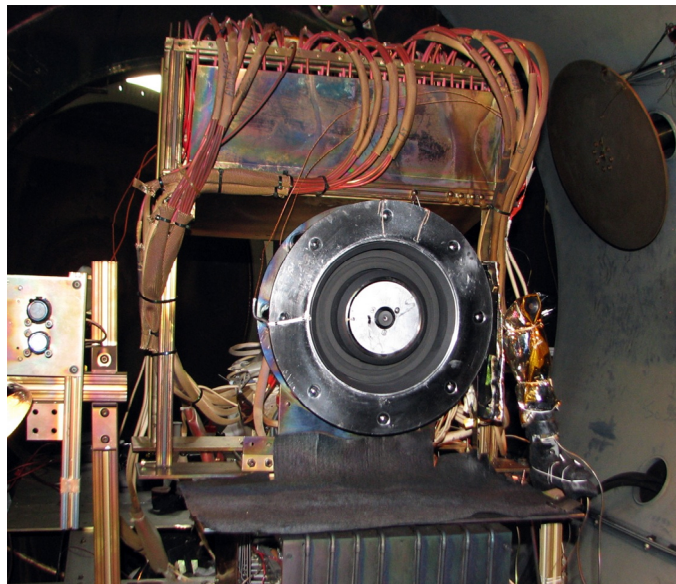


Figure 2. Graphite wall magnetically shielded H6 thruster mounted on the thrust stand in the test chamber at JPL.

control system utilized three calibrated xenon mass flow controllers and four 40-V, 19-A laboratory power supplies were used for the inner magnetic coil, outer magnetic coil, internal trim coil, and cathode heater. A 600-V, 2.6-A power supply was used for the cathode keeper. The cathode keeper and heater were turned off once the main thruster discharge was initiated. A data acquisition system was used to monitor the vacuum facility and thruster telemetry. Additional details of the test facility and power electronics can be found in Ref. [20].

The major parameters used to characterize the thruster performance are thrust, specific impulse and total efficiency. The thrust was measured directly by mounting the Hall thruster on the same inverted pendulum thrust stand that was employed in the long duration test (LDT) of the NSTAR ion thruster [33] and modified with stiffer springs and heavier weights to accommodate the higher mass of the Hall thruster. The thrust stand deflection was measured with a linear variable differential transducer (LVDT), and was calibrated by the addition of the weights simulating thrust applied to the thrust stand. In order to ensure that long-term drift did not affect the measurements by the thrust stand, calibrations were taken before and after each set of thrust measurements. The absolute uncertainty in the thrust measurement by the calibrated thrust stand is calculated to be 1%.

The specific impulse (I_{sp}) is given [5] by

$$I_{sp} = \frac{T}{\dot{m}_p g}, \quad (1)$$

where T is the measured thrust, \dot{m}_p is the total propellant mass flow rate and g is the acceleration of gravity = 9.807 m/sec². The total efficiency of the thruster is found from

$$\eta_T = \frac{1}{2} \frac{T^2}{\dot{m}_p P_T}, \quad (2)$$

where P_T is the total input power given by

$$P_T = P_d + P_{mag}.$$

In Eq. 3, P_d is the power in the discharge (discharge current times discharge voltage), and P_{mag} is the power in the electromagnets (typically 0.5-1.5% of P_d).

Ring, wall and anode temperatures inside the discharge chamber were remotely measured during these experiments using a FLIR Inframetrics PM 380 Infrared Imaging System. This camera measures the thermal radiation emitted by a surface between wavelengths of 3.4 and 5.0 μ m with a PtSi/CMOS detector. Each pixel in the detector outputs an 8 bit gray level (GL) value that corresponds to a particular temperature, depending on the emissivity of the radiating surface. Since emissivity is a material property, gray level values are calibrated by heating samples of the same materials found in the thruster with a cathode resistive heater coil and observing the samples mounted next to the thruster. A photograph of the three heated calibration samples (stainless steel (top), graphite (center), and BN (bottom)) after operation with the thruster are shown in Figure 3. Each calibration sample is insulated to avoid conductive losses and is surrounded by radiation shielding as to limit thermal emission from any other surface except the front face. A thermocouple is then inserted into each sample roughly 0.5mm from the front face in order to provide a physical measurement of the calibration surface temperature. By relating thermocouple and camera gray level values for each of the samples, calibration models can be created that allow one to accurately analyze temperatures within the actual thruster.

Since all of the calibration samples have the same surface area and radiating environment, the difference in perceived temperatures for a given camera gray level may be attributed solely to differences in surface emissivity between materials. Therefore, closer analysis of the calibration



Figure 3. Stainless steel (top), graphite (center) and boron nitride (bottom) heated samples used for camera calibration.

model for each of the materials at a fixed gray level allows one to determine the effective emissivity for each surface over the measured wavelength range. This is accomplished by comparing the total radiated power of each surface within the given spectrum to that of an ideal black body. Since the effective emissivity of BN is equal to 0.92, there exists some non-physical black body temperature that produces 8% more total radiated power than the BN surface at a given temperature. In a similar fashion, the total radiated power for the other samples can then be compared to this ideal black body in order to determine the remaining emissivities. Such a calculation yields effective emissivities of 0.70 and 0.96 for 304 Stainless Steel and Graphite respectively, which is well within the published range for these materials.

Different emissivities among materials could also potentially introduce a large source of error for such thermal imaging studies in the form of thin film effects. Throughout several hundred hours of operation, a thin black film is deposited on the surface of the H6 discharge chamber, which is believed to be sputtered, amorphous carbon from the vacuum chamber lining. The presence of such a film makes it difficult to accurately determine wall and ring temperatures given that surface emissivity will change as the film is deposited. In order to investigate this issue, a small strip of the thin black film was removed from the inner and outer walls at different azimuthal locations around the thruster. When viewed using the calibrated thermal imaging camera, these cleaned areas reveal no statistical change in perceived temperature. This most likely results from the fact that along with amorphous carbon, eroded BN from the downstream insert rings is also deposited on the channel walls. Despite its true origin, the thin black film and its effects on effective emissivity are therefore considered negligible.

III. Experimental Results

The magnetically shielded H6 Hall thruster with graphite walls was tested at power levels of 3 and 6 kW and the performance compared to that measured with the unshielded and shielded H6 thruster with BN walls. The three configurations used for comparison is shown in Figure 4: unshielded (baseline) with boron nitride rings (left); magnetically shielded with boron nitride rings (middle); and magnetically shielded with carbon rings (right). The baseline and magnetically shielded H6 configurations have each accumulated hundreds of hours of operating time, and the graphite wall thruster was operated for a total of about 10 hours to ensure that the performance was stable and the thruster was in thermal equilibrium.

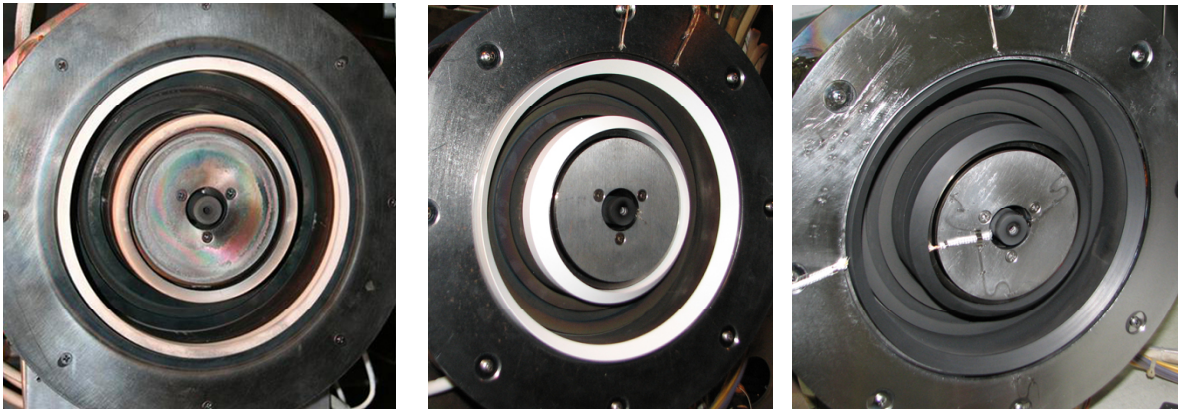


Figure 4. H6 Hall thruster with standard Boron Nitride (BN) rings (left), Magnetically Shielded (MS) BN rings (center), and MS with graphite rings (right).

A. Thruster Performance

The critical thruster performance data of interest (thrust, Isp and efficiency) were obtained for all three configurations. A comparison of these parameters and the discharge current is shown in Fig. 5 as a function of the inner magnetic field coil current. Plotting the performance results versus this coil current parameter illustrates the variation in performance with magnetic field strength near the exit plane, which is a design parameter in Hall thrusters. The plots clearly show that the magnetically shielded thruster has nearly the same efficiency as the baseline unshielded (within 2%), but the thrust is reduced and the Isp increased relative to the baseline performance. The thrust decrease was found to be due to plume divergence angle increases in the magnetically shielded configuration due to the field shape and movement of the plasma downstream by a few millimeters. The Isp

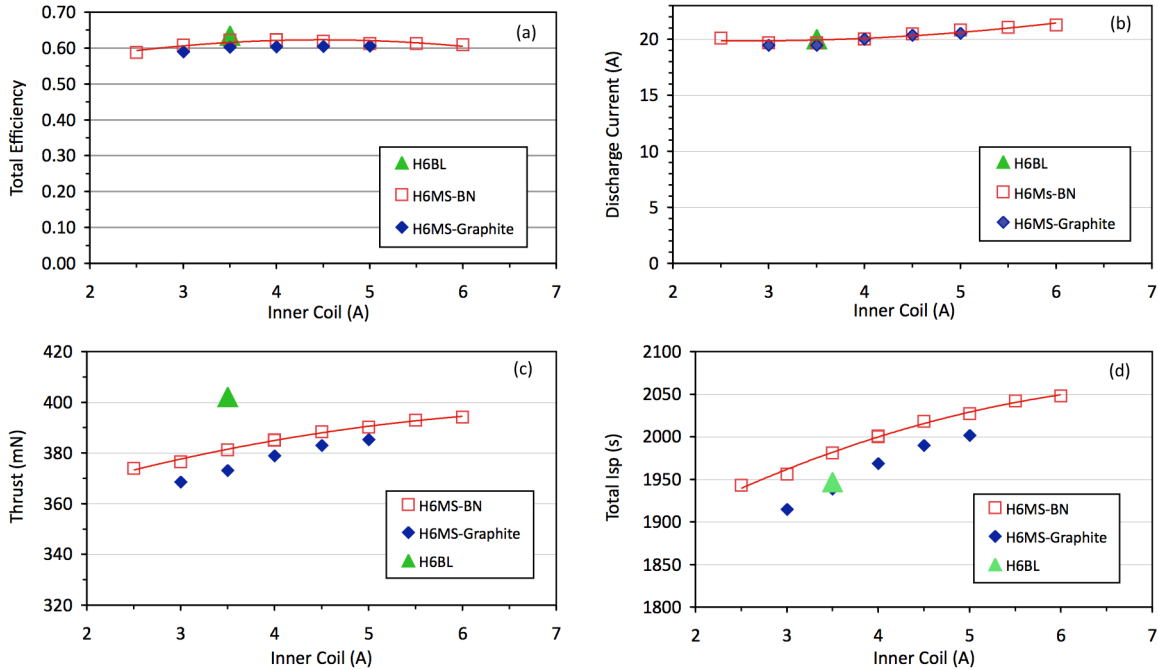


Figure 5. Thruster performance comparison for the three configurations showing, total efficiency (a), discharge current (b), thrust (c) and Isp (d) plotted against inner coil current.

increase was found to be due to a larger amount of higher ionized ions in the plume, which increase the ion velocity and therefore the Isp.

Replacement of the boron nitride rings with graphite reduced the total thruster efficiency by another 1 to 2%, to a value of about 60.5%, with similar reductions in thrust. The slight difference between the graphite wall and the boron nitride is not considered significant, and it is probable that further optimization not possible within the limited testing time available to date will make up these small differences.

It is important to emphasize the significance of these results compared to all previous attempts to change the wall material from BN or BN-based compounds to simple conductors. Figure 6 shows the results from Gascon, et.al, [10] where the thruster behavior with different wall materials was directly compared in the SPT-100 Hall thruster. Utilizing graphite discharge walls reduced the efficiency from the nominal 50% at 300 V of discharge voltage with BN-SiO₂ walls to about 30%. Conducting graphite walls produced the lowest efficiency of any of the materials tested. The use of magnetic shielding to minimize the plasma interaction with the walls removes this dependency and permits high efficiency operation (>60%) to be obtained with conducting walls.

B. Wall Temperatures and Power Level

Calibrated thermal camera measurements of the H6 discharge chamber are reported for a variety of thruster configurations and operating conditions. These values include insert ring, wall, and anode temperatures in the baseline (BL) and magnetically shielded (MS) configurations with boron nitride (BN) and graphite rings. Temperatures are given for each configuration with operating powers between 1.5kW and 6.0kW. Moreover,

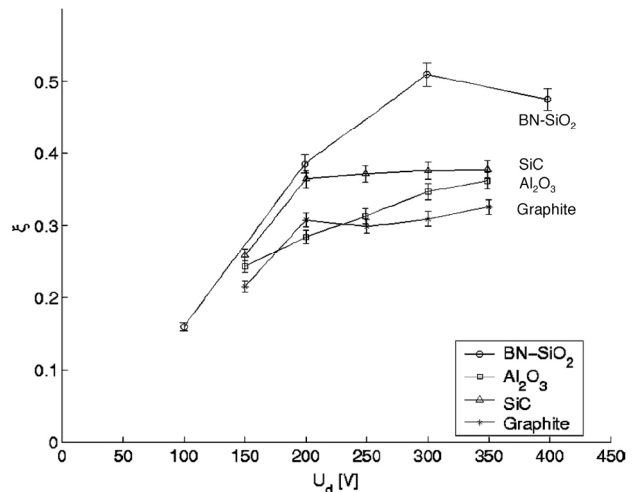


Figure 6. Comparison of the SPT-100 performance with different wall materials showing conducting graphite wall decreased the thruster efficiency to 30% at the nominal 300 V discharge voltage.

thermocouple measurements of the discharge chamber wall and insert rings have also been used to verify the camera data for the BN BL and BN MS trials.

Graphite and BN insert ring temperatures for the BL and MS configuration are shown in Fig. 7 as a function of discharge power. With the thruster operating in steady state at 6 kW, the BN ring temperatures in the MS configuration are roughly 80°C lower than the BN ring temperatures in the BL configuration. Such a reduction in ring temperature suggests that altering the magnetic field topology with magnetic shielding successfully decreases plasma bombardment of the BN rings. Moreover, the use of graphite rings instead of BN further reduces the observed ring temperatures by an additional 30°C. This is seen by the fact that the graphite ring temperatures in the MS configuration are roughly 110°C lower than the BL BN rings at 6 kW. Such a decrease in ring temperature most likely stems from the fact that the graphite rings have a slightly higher effective emissivity than the BN rings, thus allowing them to release more heat in the form of thermal radiation. Additionally, the behavior shown in Fig. 6 also suggests that changes in ring temperature are dependent on discharge power; with the use of magnetic shielding and graphite rings having a larger effect on ring temperatures at higher power densities. Such a trend therefore suggests that applying these thermal management techniques is essential for future high power Hall thruster design.

In a similar fashion, discharge chamber wall temperatures are shown in Fig. 8 for the same thruster configurations and operating conditions discussed above. The walls are located approximately in the middle of the discharge chamber length between the anode and the rings. From this data, there does not appear to be a statistical difference in wall temperatures between the MS BN and MS graphite test configurations. However, in an opposite manner from the observed changes in ring temperatures as a function of discharge power, the MS configuration with BN and graphite rings appears to cause a larger difference in discharge chamber wall temperatures at lower power densities. Additionally, these test configurations generally result in a slight increase in observed temperatures for the chamber walls, yet only at lower powers. This behavior seems to suggest that changing the magnetic field topology with magnetic shielding causes a more even distribution of thermal loads inside the discharge chamber and therefore removes the large heat flux to the insert rings as seen in the BL BN configuration.

Based on calibrated thermal camera measurements from 6 kW steady-state operation, the use of graphite rings and magnetic shielding causes an increase in outer wall temperatures of roughly 18°C while simultaneously causing a slight decrease in inner wall temperatures of roughly 5°C. The thermal behavior of the discharge chamber walls shown in Fig. 8 presents the potential trend that MS wall temperatures would be slightly lower than BL wall temperatures above operating powers of 6 kW. While this potential trend is only an extension of empirical data, it suggests that using graphite insert rings and magnetic shielding techniques could prove to be extremely useful in the future thermal design of high power Hall thrusters for operation above 6 kW.

The anode temperatures in each of the thruster configurations shown in Fig. 9 also exhibit the same thermal behavior as the discharge chamber walls for each of the operating conditions. As with the discharge chamber wall temperatures, the change in anode temperature that occurs with the use of magnetic shielding techniques and graphite rings is statistically the same between MS BN and MS graphite ring configurations. Moreover, these magnetically shielded configurations also seem to yield a larger increase in anode temperatures at

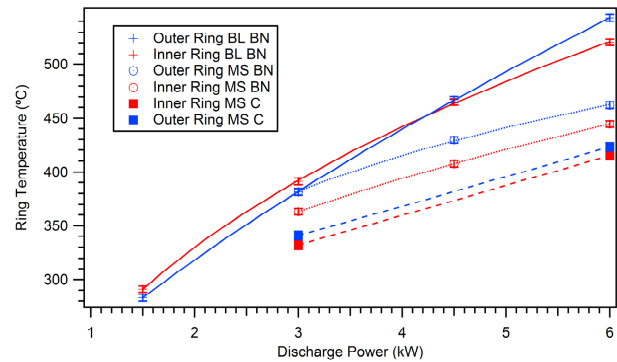


Figure 7. Ring temperatures as a function of discharge power at constant discharge voltage for the three configurations of baseline, magnetically shielded, and graphite walls.

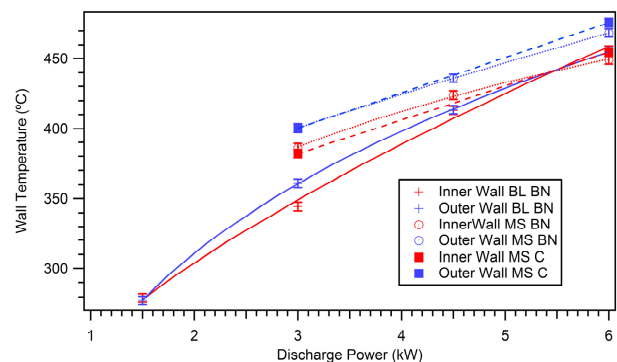


Figure 8. Discharge chamber wall temperatures (upstream of the rings) as a function of discharge power at constant discharge voltage for the three configurations of baseline, magnetically shielded, and graphite walls.

lower operating powers. The observed anode temperatures for the MS-BN and MS-graphite configurations appear to be roughly 30°C and 40°C higher than the BL-BN configuration, respectively, when operating at 6 kW in steady state. Though strictly empirical from the trends in Fig. 9, it also appears that the use of magnetic shielding techniques and graphite rings may not cause a significant decrease in anode temperatures for higher power levels unless well above 6 kW.

Using the surface temperature, emissivity, and surface geometry for the insert rings, wall, and anode, the radiated power for each of these components has been calculated and is shown in Table 2. By adding these values together, the total power radiated by the discharge chamber is calculated to be roughly 1025 W, 748 W, and 696 W for the BL-BN, MS-BN, and MS-graphite configurations respectively at 6 kW. Thus, replacing the BN insert rings with graphite rings causes a reduction in power losses due to thermal radiation by roughly 32% and reduces the radiated power from the rings by more than a factor of 2 compared to the BL BN configuration. It is posited that this number could be decreased further if the BN discharge chamber walls were also replaced with graphite in the MS configuration. Given this decrease in radiated power as well as the decrease in ring, wall, and anode temperatures at higher operating powers, it follows that the use of magnetic shielding techniques and graphite discharge chamber components should be considered for future high power Hall thruster design.

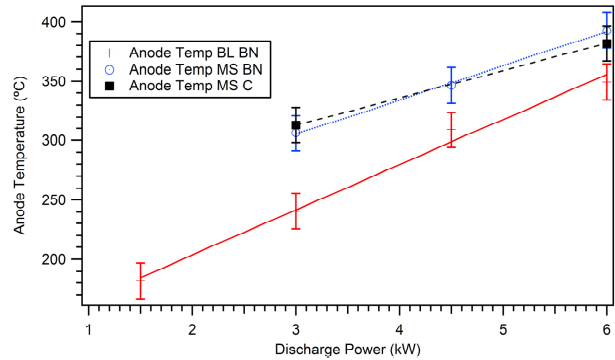


Figure 9. Anode temperatures as a function of discharge power at constant discharge voltage for the three configurations of baseline, magnetically shielded, and graphite walls.

Table 2. Radiated power for each of the discharge chamber components at the nominal 6 kW conditions.

Component	BL BN	MS BN	MS C
Anode	91 W	119 W	111 W
Inner Ring	297 W	147 W	119 W
Outer Ring	310 W	140 W	110 W
Inner Wall	98 W	95 W	98 W
Outer Wall	229 W	247 W	258 W
Total Power	1025 W	748 W	696 W

IV. Discussion

A significant observation made during these tests was that the operation and characteristics of the graphite-wall Hall thruster did not change significantly from the magnetically shielded BN configuration. The optimal magnetic field, the discharge currents and flow rates at the nominal 300 V and 6 kW were unchanged. The oscillation levels and Power Spectral Density (PSD) were similar to those observed with the magnetic shielded BN version. The discharge was stable and the thruster was turned on and throttled up in the same manner as the standard version.

Another significant observation was the potential of the rings measured during operation. It was observed that at a discharge voltage of 300 V, the floating rings self-biased to 294 ± 2 V relative to the cathode. This potential is within about one electron temperature of the plasma potentials measured near the anode and in the magnetically shielded region in front of the rings, which is consistent with the equithermal T_e distribution along the magnetic field lines from the anode region past the rings. Varying the current split between the inner and outer coils in the thruster was used to shift the plasma radially in the channel, and the floating potential of the rings responded to the increased plasma contact and higher electron temperatures during a shift toward the ring by self-biasing further away from the anode potential. Since the majority of the ions are generated in Hall thrusters in the ionization region upstream of the acceleration zone near the thruster exit plane, this self-bias of the graphite walls places them at nearly the same potential as the ion generation region. That means that the ions striking the walls gain little or no energy from the electric field in the Hall thruster that accelerates the beam ions, and so the erosion of the walls is significantly reduced compared to standard unshielded designs. The termination of the magnetic field lines on the iron pole piece on the outside of the thruster

Finally, the estimate of the total power radiated in Table 2 by the rings, walls and anode in the three configuration tested suggests that the carbon wall thruster either has significantly more thermal margin than conventional BN wall Hall thrusters, or that it can be configured to run at high power densities without overheating. Since the rings self bias to near the anode potential, it follows that an integral discharge chamber and anode

fabricated from a single piece of graphite will tend to conduct the anode power forward in the thruster to be more effectively radiated due to the better view factor to space. It is estimated that the power level might be increased a factor of two to three, or alternatively a given power thruster could be significantly reduced in size, with this new discharge chamber design.

V. Conclusion

A highly efficient, conducting wall Hall thruster has been fabricated and successfully tested. The ability to replace the ceramic (BN) walls in a traditional Hall thruster with conducting materials such as graphite is enabled by the use of the unique magnetic field tailoring near the wall, called “magnetic shielding”, that significantly reduces the plasma contact with the walls. Tests show that the conducting-wall magnetically shielded H6 thruster operated at over 60% efficiency at the nominal 300 V and 6 kW power level. The elimination of ceramic walls in Hall thrusters without significant performance penalties opens the design space for lighter, higher-power, lower-cost Hall thrusters, and represents a major advance in thruster technology.

Acknowledgments

The research described in this paper was carried out by the Jet Propulsion Laboratory, California Institute of Technology, under a contract with the National Aeronautics and Space Administration.

References

- ¹Brown et al., "Development of High-Power Electric Propulsion Technology for Near-Term and Mid-Term Space Power," JANNAF-1193, 2010.
- ²N. Strange et al., "Solar Electric Propulsion for a Flexible Path of Human Space Exploration," IAC-10.A5.2.4, 2010.
- ³D.Y. Oh, "Evaluation of Solar Electric Propulsion Technologies for Discovery Class Missions", AIAA-2005-4270, 41st Joint Propulsion Conference, Tucson, Az, July 10-13, 2005.
- ⁴R.R. Hofer, T.M. Randolph, D.Y. Oh, J.S. Snyder, "Evaluation of a 4.5 kW Commercial Hall Thruster System for NASA Science Missions", AIAA-2006-4469, 42nd Joint Propulsion Conference, Sacramento, CA, July 9-12, 2006.
- ⁵D.M. Goebel and I. Katz, *Fundamentals of Electric Propulsion; Ion and Hall Thrusters*, John Wiley and Sons, NJ 2008.
- ⁶Y. Raitses, D. Staack, A. Dunaevsky, and N. J. Fisch, "Operation of a segmented Hall thruster with low-sputtering carbon-velvet electrodes," *J. Appl. Phys.*, **99** (3), pp. 036103-1–036103-3, Feb. 2006.
- ⁷Y. Raitses, M. Keidar, D. Staack and N. J. Fisch, "Effects of segmented electrode in Hall current plasma thrusters", *J. Appl. Physics*, **92** (9), 4906-4911, 2002.
- ⁸Y. Raitses, D. Staack, and N. J. Fisch, "Controlling the plasma potential distribution in segmented Hall thruster," *IEEE Trans. Plasma Sci.*, **36** (4), pp. 1202–1203, Aug. 2008.
- ⁹Y. Raitses, J. Ashkenazy, G. Appelbaum, and M. Guelman, "Experimental investigation of the effect of channel material on Hall thruster characteristics," IEPC Paper 97-056, 25th Int. Electric Propulsion Conf., Cleveland, OH, Aug., 1997.
- ¹⁰N. Gascon, M. Dudeck, and S. Barral, "Wall material effects in stationary plasma thrusters I: Parametric studies of an SPT-100," *Phys. Plasmas*, **10** (10), pp. 4123–4136, Oct. 2003.
- ¹¹S. Barral, K. Makowski, Z. Peradzynski, N. Gascon, and M. Dudeck, "Wall material effects in stationary plasma thrusters II. Near-wall and in-wall conductivity," *Phys. Plasmas*, **10** (10), pp. 4137–4152, Oct. 2003.
- ¹²D. Staack, Y. Raitses, and N. J. Fisch, "Control of acceleration region in Hall thrusters," IEPC Paper 03-0273, 28th Int. Electric Propulsion Conf., Toulouse, France, Mar., 2003.
- ¹³A. Dunaevsky, Y. Raitses, and N. J. Fisch, "Secondary electron emission from dielectric materials of a Hall thruster with segmented electrodes", *Physics of Plasmas*, **10** (6), 2574-2577, 2003.
- ¹⁴Y. Raitses, A. Smirnov, D. Staack, and N. J. Fisch, "Measurements of secondary electron emission effects in Hall thrusters," *Phys. Plasmas*, **13** (1), pp. 014502-1–014502-4, Jan. 2006.
- ¹⁵Y. Raitses, et al. "Effect of Secondary Electron Emission on Electron Cross-Field Current in *ExB* Discharges" *IEEE T-PS*, **39**, pp. 995-1006, (2011).
- ¹⁶K.deGrys, A. Mathers, B. Welander, V. Khayms, "Demonstration of 10,400 Hours of Operation on a 4.5 kW Qualification Model Hall Thruster", 46st Joint Propulsion Conference, Nashville, TN, July 25-28, 2010.
- ¹⁷I. G. Mikellides, I. Katz, R.R. Hofer, D.M. Goebel, K. deGrys and A. Mathers, "Magnetic Shielding of the Acceleration Channels Walls in a Long-Life Hall Thruster", AIAA-2010-6942, 46th Joint Propulsion Conference and Exhibit, Nashville, TN, July 25-28, 2010.
- ¹⁸I.G. Mikellides, I. Katz, R.R. Hofer, D.M. Goebel, and K. deGrys, "Magnetic Shielding of the Channel Walls in a Hall Plasma Accelerator", *Physics of Plasmas*, **18**, 033501 (2011).
- ¹⁹I.G. Mikellides, I. Katz, R.R. Hofer, and D.M. Goebel, "Design of a Laboratory Hall Thruster with Magnetically Shielded Channel Walls, Phase I: Numerical Simulations," AIAA-2011-5809, 47th Joint Propulsion Conference and Exhibit, San Diego, CA, July 31-Aug 3, 2011.

- ²⁰R.R. Hofer, D.M. Goebel, I.G. Mikellides and I. Katz, "Design of a Laboratory Hall Thruster with Magnetically Shielded Channel Walls, Phase II: Experiments", AIAA-2012-3788, 48th AIAA/ASME/SAE/ASEE Joint Propulsion Conference and Exhibit, Atlanta, Georgia, July 30-1, 2012.
- ²¹I. G. Mikellides, I. Katz, R. R. Hofer, D. M. Goebel, "Design of a Laboratory Hall Thruster with Magnetically Shielded Channel Walls, Phase III: Comparison of Theory with Experiment", AIAA-2012-3789, 48th AIAA/ASME/SAE/ASEE Joint Propulsion Conference and Exhibit, Atlanta, Georgia, July 30-1, 2012
- ²²I.G. Mikellides, I. Katz, R.R. Hofer, D.M. Goebel, "Magnetic Shielding of Walls from the Unmagnetized Ion Beam in a Hall Thruster", *Appl.Phys.Lett.*, **102**, 023509 (2013).
- ²³J.M. Haas, R.R. Hofer, D.L. Brown, B.M. Reid, and A.D. Gallimore, "Design of the H6 Hall Thruster for High Thrust/Power Investigation," Presented at the 54th JANNAP Propulsion Meeting, Denver, CO, May 14-17, 2007.
- ²⁴D.M. Goebel and R.M. Watkins, "Compact Lanthanum Hexaboride Hollow Cathode", *Rev. Sci. Instrum.*, **81**, 083504, (2010).
- ²⁵D.L. Brown, B.M. Reid, and A.D. Gallimore, R.R. Hofer, J.M. Haas, and C.W. Larson, "Performance Characterization and Design Verification of the H6 Laboratory Model Hall Thruster," Presented at the 54th JANNAP Propulsion Meeting, Denver, CO, May 14-17, 2007.
- ²⁶Brown, D. L., Larson, C. W., Beal, B. E., and Gallimore, A. D., "Methodology and Historical Perspective of a Hall Thruster Efficiency Analysis," *Journal of Propulsion and Power* 25, 6, 1163-1177 (2009).
- ²⁷Huang, W., Gallimore, A. D., and Hofer, R. R., "Neutral Flow Evolution in a 6-kW Hall Thruster," *Journal of Propulsion and Power* 27, 3, 553-563 (2011).
- ²⁸Shastry, R., Gallimore, A. D., and Hofer, R. R., "Experimental Characterization of the near-Wall Plasma in a 6-kW Hall Thruster and Comparison to Simulation," AIAA Paper 2011-5589, July 2011.
- ²⁹R.R. Hofer, I. Katz, I. G. Mikellides, D.M. Goebel, K.K. Jameson, R.M. Sullivan, and L.K. Johnson, "Efficacy of Electron Mobility Models in Hybrid-PIC Hall Thruster Simulations", AIAA 2008-4924, 44th AIAA Joint Propulsion Conference, Hartford, CT, July 21 – 23, 2008.
- ³⁰D.M.Goebel, K.K.Jameson and R.R. Hofer, "Hall Thruster Cathode Flow Impacts on Cathode Coupling and Cathode Life", *J. of Propulsion and Power*, **28**, No.2, pp.355-363, (2012).
- ³¹A. Sengupta, J.R. Anderson, C. Garner, J.R. Brophy, K. deGroh, B. Banks, and T. Thomas, "Deep Space 1 Flight Space Ion Thruster 30,000 hour Life Test", *Journal of Propulsion and Power*, **25**, p. 105-117 (2009).
- ³² R. R. Hofer, L. K. Johnson, D. M. Goebel, and R.E. Wirz, "Effects of Internally-Mounted Cathodes on Hall Thruster Plume Properties," *IEEE Transactions on Plasma Science* 36, 5, 2004-2014 (2008).
- ³³J.E. Polk, J.R. Anderson, J.R. Brophy, V.K. Rawlin, M.J. Patterson, J. Sovey and J. Hamley, "An Overview of the Results from an 8200 Hour Wear Test of the NSTAR Ion Thruster", AIAA-1999-2446, 35th Joint Propulsion Conference, Los Angeles, CA, June 20-24, 1999.